AIAA 80-1439R

Calculation of Turbulent Boundary Layers with Separation and Viscous-Inviscid Interaction

D. L. Whitfield*
Mississippi State University, Starksville, Miss.
T. W. Swafford†
ARO, Inc., Arnold Air Force Station, Tenn.
and
J. L. Jacocks‡
Calspan Field Services, Inc., Arnold Air Force Station, Tenn.

A method is presented for calculating turbulent boundary layers with separation, reattachment, and viscous-inviscid interaction. The boundary-layer method is a two-dimensional planar or axisymmetric inverse integral technique based on an analytical description of attached and separated turbulent boundary-layer velocity profiles. The inviscid region is calculated using a time-dependent, three-dimensional, finite-volume Euler equation code. Viscous-inviscid interaction is achieved using the surface source model. Transonic viscous-inviscid interacting flows over planar, axisymmetric, and three-dimensional configurations are calculated and compared with experimental data.

Nomenclature

A = cell face area vector
a,b = parameter defined by steps 8 and 7, respectively, of Table 1
c = speed of sound
c_f = local skin friction coefficient, $2\tau_w/\rho_e u_e^2$
$\tilde{c}_f$ = $F_c c_f$
C_p = pressure coefficient, $2(P-P_\infty)/\rho_\infty u_\infty^2$
D = shear-work integral, $= \int_0^\infty \frac{\tau}{\tau_w}\frac{\partial}{\partial y}\left(\frac{u}{u_e}\right)dy$
e = total energy, $e=[P/(\gamma-1)]+\frac{1}{2}\rho(u^2+v^2+w^2)$
F = flux tensor, defined by Eq. (12b)
F_c = $[1+(\gamma-1)M_e^2/2]^{\frac{1}{2}}$
G = vector of conserved gasdynamic variables, defined by Eq. (12a)
g = function defined by steps 5 and 6 of Table 1
$\bar{H}$ = incompressible shape factor, defined by Eq. (4)
H_{δ^*} = shape factor based on δ^*, defined by Eq. (1)
$H_{\delta^{**}}$ = shape factor based on δ^{**}, defined by Eq. (3)
H_{θ^*} = shape factor based on θ^*, defined by Eq. (2)
k = index which is zero for planar flow and one for axisymmetric flow
ℓ = body length
M = Mach number
n = unit normal vector
P = pressure
q = velocity vector
r_w = local body radius
Re_θ = local momentum thickness Reynolds number, $u_e\theta/\nu_e$
$\overline{Re_\theta}$ = Re_θ/F_c
S = magnitude of A
s = parameter defined by step 2 of Table 1
t = time
u,v,w = Cartesian velocity components, except in the boundary-layer equations where u is taken to be parallel to body surface
u^+ = boundary-layer velocity coordinate, $=u/u_\tau$
u_τ = friction velocity, $=u_e(|c_f|/2)^{\frac{1}{2}}$
Vol = cell volume
W = smoothing factor, defined by Eq. (18)
x,y,z = Cartesian coordinates, except in the boundary-layer equations where x and y are parallel and normal to the body surface, respectively
y^+ = boundary-layer y coordinate, $=u_\tau y/\nu$
α = variable defined by Eq. (9)
β = variable defined by Eq. (10)
γ = ratio of specific heats
δ^* = boundary-layer displacement thickness, $= \int_0^\infty \left(1-\frac{\rho u}{\rho_e u_e}\right)dy$
δ^{**} = boundary-layer density thickness, $= \int_0^\infty \frac{u}{u_e}\left(1-\frac{\rho}{\rho_e}\right)dy$
$\tilde{\delta}^*$ = equivalent incompressible displacement thickness, $= \int_0^\infty \left(1-\frac{\tilde{u}}{\tilde{u}_e}\right)dy$
θ = boundary-layer momentum thickness, $= \int_0^\infty \frac{\rho u}{\rho_e u_e}\left(1-\frac{u}{u_e}\right)dy$
$\tilde{\theta}$ = equivalent incompressible momentum thickness, $= \int_0^\infty \frac{\tilde{u}}{\tilde{u}_e}\left(1-\frac{\tilde{u}}{\tilde{u}_e}\right)dy$

Presented as Paper 80-1439 at the AIAA 13th Fluid and Plasma Dynamics Conference, Snowmass, Colo., July 14-16, 1980; submitted Sept. 24, 1980; revision received March 26, 1981.

*Professor of Aerospace Engineering. Member AIAA.
†Research Engineer, Engine Test Facility, AEDC Group. Member AIAA.
‡Supervisor, Propulsion Wind Tunnel Facility, AEDC Division. Member AIAA.

θ^* = boundary-layer energy thickness,

$$= \int_0^\infty \frac{\rho u}{\rho_e u_e}\left(1 - \frac{u^2}{u_e^2}\right)dy$$

ν = kinematic viscosity
ρ = density
τ = total shear stress (molecular + turbulent)

Subscripts

bc = boundary condition
c = airfoil chord length
D = body diameter
e = boundary-layer edge
i = inviscid
ℓ = body length
n = normal to surface
v = viscous
w = wall
∞ = infinity or freestream

Superscripts

η = time index
$\bar{()}$ = low-speed or incompressible value; also, predicted value as used in Eq. (14)

Introduction

SUCCESSFUL application of computational fluid dynamics to the design and analysis of flight vehicles depends on the successful treatment of viscous-inviscid interacting flow. Significant progress is being made in the solution of time-dependent, ensemble-averaged Navier-Stokes equations for compressible turbulent flow. The Navier-Stokes approach, however, is presently too expensive for much of the technical community and, although complex flows can be solved, further advances in numerical techniques and computer technology are needed before this approach can be used routinely.

In the interim, problems involving viscous-inviscid interaction with and without separation are commonplace and must be confronted. One approach to solve these problems is to use an inviscid solution for the region away from the body, a viscous solution near the body, and match the two at some location and in some fashion. Besides the problem of where and how to match these solutions is the problem of dealing with the singularity in the boundary-layer equations at the point of separation if the pressure is prescribed as a boundary condition in the usual direct method of calculation.[1] Catherall and Mangler[2] demonstrated that this singularity can be removed by prescribing the displacement thickness or the wall shear-stress distribution in place of the pressure distribution. This is the so-called inverse boundary-layer method. With the singularity removed, the remaining problems are: 1) the computation of turbulent boundary layers with separation, 2) the coupling of the viscous and inviscid regions, and 3) a rational, a priori means of specifying the displacement thickness or the wall shear-stress distribution for the inverse boundary-layer calculation. The purpose of the present paper is to present a method of calculating turbulent boundary layers with and without separation, and to couple the boundary-layer method with an inviscid Euler equation code to obtain solutions for flows with viscous-inviscid interaction.

Several inverse turbulent boundary-layer calculation techniques have been presented, e.g., Kuhn and Nielsen,[3] Thiede,[4] East et al.,[5] and Carter.[6] The method of Carter[6] is a finite-difference technique, whereas those of Kuhn and Nielsen[3] and Thiede[4] are moment of momentum integral equation methods, and East et al.[5] is a lag-entrainment integral method. The boundary-layer method described in this paper is a mean-flow kinetic energy integral equation method that differs from other integral methods in the use of an analytically described turbulent boundary-layer velocity profile for both attached and separated flow. The velocity profile expression is used to establish the necessary correlation parameters and also is used to evaluate the dissipation integral term as opposed to using an empirically derived dissipation coefficient.

Kuhn,[7] Thiede,[4] and Carter[8] have combined their boundary-layer methods with inviscid flow calculation methods to compute flows with viscous-inviscid interaction. Kuhn[7] uses a displacement surface as an effective boundary for the inviscid flow. This displacement surface is assumed conical (for axisymmetric bodies) in separated regions. In the boundary-layer calculation, the boundary-layer edge velocity is prescribed upstream and downstream of separation, and the displacement thickness is prescribed in the separated region. Thiede[4] combines viscous and inviscid flows by tangential coupling along the boundary-layer displacement thickness for weak interaction problems, and tangential and normal velocity coupling along the boundary-layer edge for strong interaction problems.

Carter[8] recently introduced a viscous-inviscid iteration procedure that is extremely attractive. This method uses the surface source model of the type originally proposed by Lighthill[9] and used by Lock,[10] for example. The key feature of Carter's[8] work is the method suggested for updating the displacement thickness that is required in the expression for calculating the surface source term. Carter's iteration procedure[8] is easy to implement and is used in the present work.

The inviscid flow computational methods used in Refs. 6-8 solve the nonconservative potential flow equations. In the present work a fully conservative, time-dependent, three-dimensional, finite volume, Euler equation code is used. In this regard, the surface source model, which involves the specification of the velocity normal to the wall in the inviscid calculation, is a convenient approach because, in contrast to an effective surface displacement approach, the inviscid flow computational mesh remains fixed with respect to the actual body geometry. The surface source term for the inviscid calculations is then updated in time by periodically solving the inverse boundary-layer problem.

In this paper the inverse turbulent boundary-layer method for calculating attached or separated flows is described and comparisons are made between calculated and measured turbulent separated boundary-layer data. The Euler equation code is then described followed by a description of the method used to treat viscous-inviscid interaction. Finally, comparisons between calculated and measured viscous-inviscid interacting flows are presented and discussed.

Turbulent Boundary-Layer Calculation Method

The turbulent boundary-layer calculation method presented herein is an extension of the method presented in Ref. 11 for attached flow. The key feature of the method of Ref. 11 was the use of a new representation of the turbulent boundary-layer velocity profile.[12] The current method is a further extension of the results of Ref. 12 to include velocity profiles in separated flow. This allows for the development of auxiliary relations necessary for calculating turbulent boundary layers with separation.

Velocity Profile Representation

The equation used to describe analytically both attached and separated turbulent boundary-layer velocity profiles was derived by Swafford.[13] Similar to the expression for attached flow,[12] the equation derived in Ref. 13 is the sum of two transcendental functions, one expressed in terms of the inner variable $\bar{y}^+$ and one expressed in terms of the outer variable $y/\bar{\theta}$. The essential feature of the modification of the attached-flow equation was to allow for a negative velocity slope near the wall for separated boundary layers. Table 1 is a summary of the procedure for computing both attached and separated

Table 1 Procedure for computing separated or attached turbulent boundary-layer velocity profiles

Step	Requirement	Comment
1	$\bar{H}$, $\bar{u}_e^+$, and $\overline{Re_\theta}$ are inputs	$\bar{u}_e^+ = (2/\lvert\bar{c}_f\rvert)^{1/2}$
2	Compute $s = \bar{c}_f/\lvert\bar{c}_f\rvert$	$\bar{c}_f = \bar{c}_f(\overline{Re_\theta}, \bar{H})$
3	Compute $\frac{\bar{u}}{\bar{u}_e}(2) = \frac{1}{1.95}\left[\tanh^{-1}\left(\frac{8.5-\bar{H}}{7.5}\right) - 0.364\right]$	$\frac{\bar{u}}{\bar{u}_e}\left(\frac{y}{\bar{\theta}}\right)$ at $\frac{y}{\bar{\theta}} = 2$
4	Compute $\frac{\bar{u}}{\bar{u}_e}(5) = 0.155 + 0.795\ \text{sech}\,[0.51(\bar{H}-1.95)]$	$\frac{\bar{u}}{\bar{u}_e}\left(\frac{y}{\bar{\theta}}\right)$ at $\frac{y}{\bar{\theta}} = 5$ $\text{sech}(z) = \frac{1}{\cosh(z)} = \frac{2}{e^z + e^{-z}}$
5	Compute $g(2) = \left[\frac{\bar{u}}{\bar{u}_e}(2) - \frac{s}{0.09\bar{u}_e^+}\tan^{-1}\left(\frac{0.18\overline{Re_\theta}}{\bar{u}_e^+}\right)\right]\Big/\left[1 - \frac{s\pi}{0.18\bar{u}_e^+}\right]$	$g\left(\frac{y}{\bar{\theta}}\right)$ at $\frac{y}{\bar{\theta}} = 2$
6	Compute $g(5) = \left[\frac{\bar{u}}{\bar{u}_e}(5) - \frac{s}{0.09\bar{u}_e^+}\tan^{-1}\left(\frac{0.45\overline{Re_\theta}}{\bar{u}_e^+}\right)\right]\Big/\left[1 - \frac{s\pi}{0.18\bar{u}_e^+}\right]$	$g\left(\frac{y}{\bar{\theta}}\right)$ at $\frac{y}{\bar{\theta}} = 5$
7	Compute $b = \ell n\left\{\frac{\tanh^{-1}[g^2(2)]}{\tanh^{-1}[g^2(5)]}\right\}\Big/\ell n(2/5)$	$\tanh^{-1}(z) = \frac{1}{2}\ell n\left(\frac{1+z}{1-z}\right)$
8	Compute $a = \frac{\tanh^{-1}[g^2(2)]}{2^b}$	$\tanh(z) = \frac{e^{2z}-1}{e^{2z}+1}$
9	$\bar{u}^+ = \frac{s}{0.09}\tan^{-1}(0.09\bar{y}^+) + \left(\bar{u}_e^+ - \frac{s\pi}{0.18}\right)\tanh^{1/2}\left[a\left(\frac{y}{\bar{\theta}}\right)^b\right]$	$\frac{\bar{u}}{\bar{u}_e} = \frac{u}{u_e} = \frac{\bar{u}^+}{\bar{u}_e^+}$ $\bar{y}^+ = \frac{\overline{Re_\theta}}{\bar{u}_e^+}\cdot\frac{y}{\bar{\theta}}$

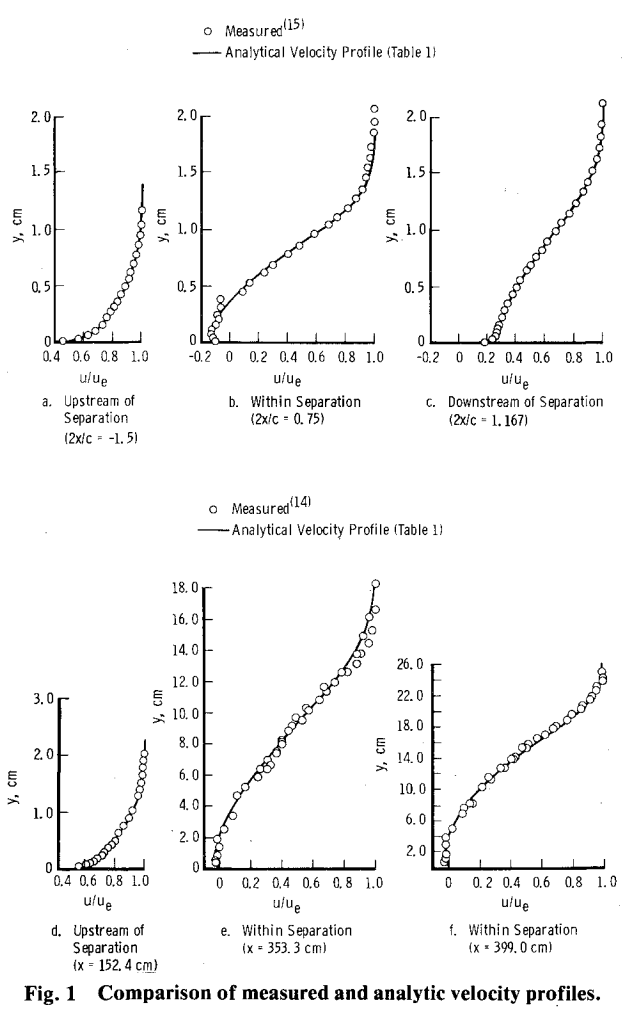

Fig. 1 Comparison of measured and analytic velocity profiles.

turbulent boundary-layer velocity profiles. The velocity profile expression is valid over the entire domain $0 \le y < \infty$, and is given as step 9 in Table 1.

Figure 1 shows comparisons of the analytical velocity profile representation with the low-speed experimental data of Simpson et al.[14] and the transonic data of Alber et al.[15] for attached, separated, and reattached boundary layers. These data were used to establish the necessary correlations for separated flow which are given as steps 3 and 4 in Table 1. The means used for relating compressible and incompressible variables are given in Ref. 13.

Auxiliary Relation Correlations

An analytical expression for attached and separated turbulent boundary-layer velocity profiles permits the evaluation of certain auxiliary correlations necessary for the inverse integral boundary-layer calculation method. There are four integral length scales associated with the integral boundary-layer equations: δ^*, θ, θ^*, and δ^{**}. The approach taken in Ref. 11 was to define the shape factors

$$H_{\delta^*} = \delta^*/\theta \tag{1}$$

$$H_{\theta^*} = \theta^*/\theta \tag{2}$$

$$H_{\delta^{**}} = \delta^{**}/\theta \tag{3}$$

and then correlate these shape factors with M_e and $\bar{H}$, where $\bar{H}$ is defined as

$$\bar{H} = \delta^*/\bar{\theta} \tag{4}$$

However, only the $H_{\theta^*} = f(\bar{H})$ correlation for $M_e \approx 0$ (for $M_e \approx 0$, $H_{\delta^*} \approx \bar{H}$, and $H_{\delta^{**}} \approx 0$) was evaluated for separated flow because of the lack of separated flow data with significant compressibility. Figure 2 shows the $H_{\theta^*} = f(\bar{H})$ correlation taken from Ref. 13.

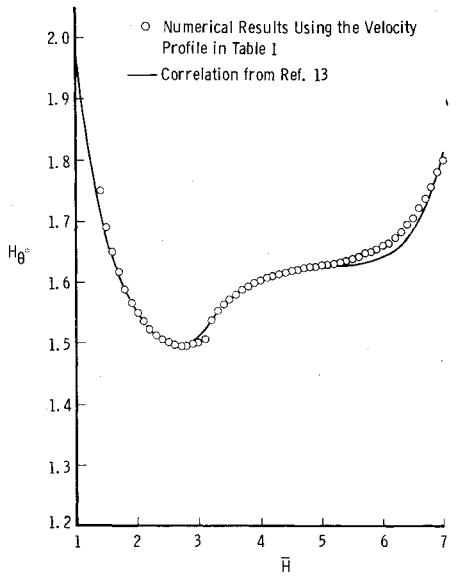

Fig. 2 Correlation of H_{θ^*} for adiabatic, incompressible flow.

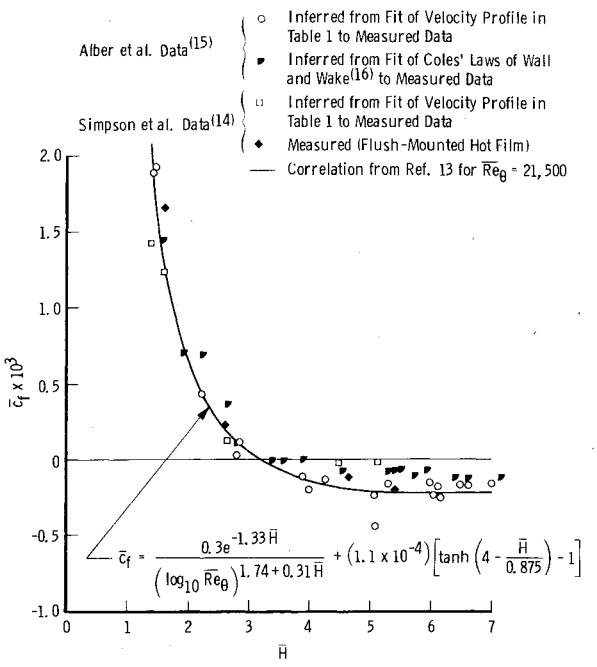

Fig. 3 Correlation of $\bar{c}_f$ for adiabatic, incompressible flow.

The correlations for H_{δ^*}, H_{θ^*}, $H_{\delta^{**}}$, and $\theta/\bar{\theta}$ obtained in Ref. 11 are functions not only of $\bar{H}$, but also Mach number. In the present method, the correlations developed in Ref. 11 for H_{δ^*}, $H_{\delta^{**}}$, and $\theta/\bar{\theta}$ are retained because of their Mach number dependence. However, these relationships must be considered tentative for large shape factors because of the lack of compressible separated flow data.

In addition to the shape factor correlation, an expression for skin friction valid for both attached and separated flow is needed. An expression was derived in Ref. 13 from skin friction data which were inferred from curve fits using the velocity profile equation given in Table 1, curve fits of Coles' law-of-the-wall and law-of-the-wake,[16] and measured skin friction data.[14] The second term of the skin friction correlation shown in Fig. 3 was selected such that for shape factors less than about 2.3, the expression degenerates into the skin friction relation given by White[17] (Eq. 6-179).

Calculation Method

The momentum and mean-flow kinetic energy integral equations[11] can be written

$$\frac{1}{r_w^k \rho_e u_e^2}\frac{\mathrm{d}}{\mathrm{d}x}(r_w^k \rho_e u_e^2 \theta) + H_{\delta^*}\frac{\theta}{u_e}\frac{\mathrm{d}u_e}{\mathrm{d}x} = \frac{c_f}{2} \tag{5}$$

$$\frac{1}{2r_w^k \rho_e u_e^3}\frac{\mathrm{d}}{\mathrm{d}x}(r_w^k \rho_e u_e^3 \theta H_{\theta^*}) + H_{\delta^{**}}\frac{\theta}{u_e}\frac{\mathrm{d}u_e}{\mathrm{d}x} = \frac{c_f}{2}D \tag{6}$$

Equations (5) and (6) can be recast into the form

$$\frac{\mathrm{d}\bar{H}}{\mathrm{d}x} = \left[1\Big/\left(\alpha + \frac{\beta}{H_{\delta^*}}\frac{\mathrm{d}H_{\delta^*}}{\mathrm{d}\bar{H}}\right)\right]\left[\frac{|c_f D|}{\theta H_{\theta^*}} - \beta\frac{c_f}{2\theta} - \frac{1-\beta}{r_w^k \delta^*}\frac{\mathrm{d}}{\mathrm{d}x}(r_w^k \delta^*)\right] \tag{7}$$

$$\frac{\mathrm{d}M_e}{\mathrm{d}x} = \left\{\frac{M_e[1+(M_e^2/5)]}{2+H_{\delta^*}-M_e^2}\right\}\left\{\frac{c_f}{2\theta} + \frac{1}{H_{\delta^*}}\left(\frac{\mathrm{d}H_{\delta^*}}{\mathrm{d}\bar{H}}\right)\frac{\mathrm{d}\bar{H}}{\mathrm{d}x} - \frac{1}{r_w^k \delta^*}\frac{\mathrm{d}}{\mathrm{d}x}(r_w^k \delta^*)\right\} \tag{8}$$

where

$$\alpha = \frac{1}{H_{\theta^*}}\frac{\mathrm{d}H_{\theta^*}}{\mathrm{d}\bar{H}} - \frac{1}{H_{\delta^*}}\frac{\mathrm{d}H_{\delta^*}}{\mathrm{d}\bar{H}} \tag{9}$$

$$\beta = \frac{3+2(H_{\delta^{**}}/H_{\theta^*})-M_e^2}{2+H_{\delta^*}-M_e^2} \tag{10}$$

Given the velocity profile of step 9 in Table 1, the correlations shown in Figs. 2 and 3, and r_w and δ^* distributions, Eqs. (7) and (8) represent two equations for the two unknowns, $\bar{H}$ and M_e. A Runge-Kutta method was used to solve the system of equations.

The dissipation integral D is evaluated using the Cebeci-Smith two-layer eddy viscosity turbulence model[18] for τ, and the analytical velocity profile expression for $\partial u/\partial y$. The dissipation integral is, therefore, calculated at each streamwise location as opposed to using an empirical dissipation integral coefficient.

Calculated Results

Unfortunately, relatively little separated turbulent boundary-layer data were found to test the present method of calculation. However, comparisons of computed results and measured data from two low-speed flows are presented.

Figure 4 gives comparisons of measured and computed distributions of u_e, θ, c_f, and H for the Simpson et al.[14] flow. The agreement is reasonably good upstream of separation ($x \cong 3.2$ m). For $x > 3.2$ m, agreement between measured data and calculation is not as good as for $x < 3.2$ m, with the exception of the skin friction. The same sort of agreement was also obtained by East et al.[5] using a lag-entrainment method. The calculations of East et al.,[5] however, were performed using the direct method to some point upstream of separation, and the inverse method downstream of that point. In the present calculations, the inverse method is used throughout and no switching occurs between direct and inverse methods.

Figure 5 presents comparisons of the present calculations and the low-speed measurements of Chu and Young[19] for M_e, θ, c_f, and H. Reasonably good agreement between measurements and calculations is obtained for the entire range of x, even for $x \geq 1.68$ m where the state of the boundary layer is changing rapidly.

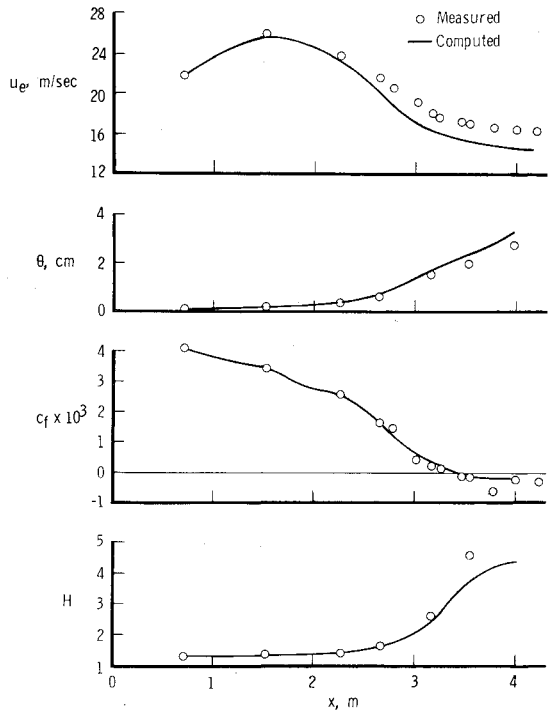

Fig. 4 Present computations and low-speed measurements of Simpson et al.[14]

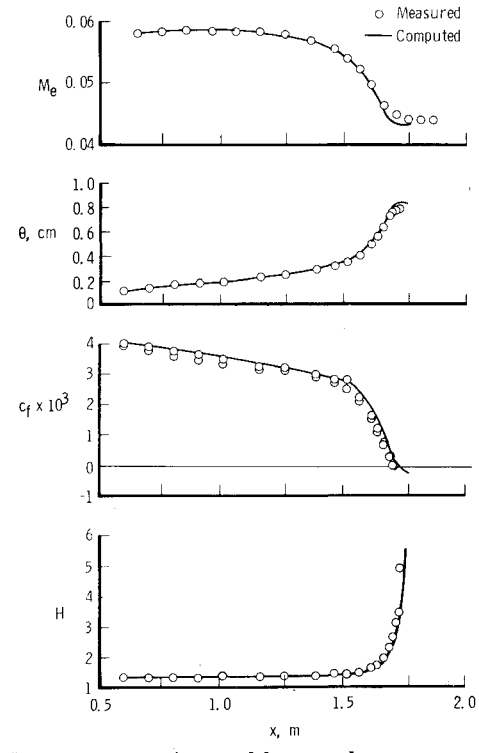

Fig. 5 Present computations and low-speed measurements of Chu and Young.[19]

Euler Equation Calculation Method

The three-dimensional unsteady Euler equations are written in Cartesian coordinates as

$$\frac{\partial G}{\partial t} + \nabla \cdot F = 0 \tag{11}$$

where

$$G = \begin{bmatrix} \rho \\ \rho u \\ \rho v \\ \rho w \\ e \end{bmatrix} \tag{12a}$$

$$F = \begin{bmatrix} \rho u & \rho v & \rho w \\ \rho u^2 + P & \rho uv & \rho uw \\ \rho uv & \rho v^2 + P & \rho vw \\ \rho uw & \rho vw & \rho w^2 + P \\ (e+P)u & (e+P)v & (e+P)w \end{bmatrix} \tag{12b}$$

and

$$e = \frac{P}{\gamma - 1} + \frac{1}{2}\rho(u^2 + v^2 + w^2) \tag{12c}$$

These equations are rewritten in a finite-volume formulation and the divergence theorem applied to yield

$$\frac{\partial G}{\partial t} = -\frac{1}{\text{Vol}} \int_S F \cdot n \, dS \tag{13}$$

The solution algorithm adopted for Eq. (13) is the predictor-corrector technique of MacCormack.[20] As applied to an arbitrary volume element with face area vectors denoted by A, the MacCormack scheme advances the solution in time from G^η to $G^{\eta+1}$ by

$$\bar{G}^{\eta+1} = G^\eta - \frac{\Delta t}{\text{Vol}} \sum_S F^\eta \cdot A_f \tag{14a}$$

$$G^{\eta+1} = \frac{1}{2}\left[G^\eta + \bar{G}^{\eta+1} - \frac{\Delta t}{\text{Vol}} \sum_S \bar{F}_b^{\eta+1} \cdot A_b\right] \tag{14b}$$

where the time step is limited by the Courant-Friedrich-Lewy linear stability criterion

$$\Delta t \le \left.\frac{\text{Vol}}{|q \cdot A| + cS}\right|_{\min} \tag{15}$$

The subscripts f and b in Eq. (14) represent forward and backward permutation of local indices.

Boundary conditions are treated using phantom grid points exterior to the computational domain. The inflow and outer boundary points are maintained at freestream conditions whereas the downstream outflow boundary uses zero gradients. At planes of symmetry mirror conditions are used. Pressure, density, and energy at the phantom points are set equal to the neighboring interior values and the flux vector mirrored using

$$\rho q_{bc} = \rho q - 2[\rho q \cdot A / S^2]A \tag{16}$$

where A is the boundary area vector. For viscous surfaces, the normal mass flux ρv_n obtained from the boundary-layer solution was applied using

$$\rho q_{bc} = \rho q - 2\left[\frac{\rho q \cdot A}{S^2} + \frac{(\rho v)_n n \cdot A}{S^2}\right]A \tag{17}$$

with zero-normal gradients on pressure, density, and energy.

Initial conditions are uniform freestream conditions with the body impulsively introduced at time zero. This distur-

bance, in association with irregular volume elements, requires that some form of artificial viscosity be added to the MacCormack scheme to suppress a nonlinear instability. An explicit smoothing technique is currently used which consists of an average of neighboring points with the center point weighted with the factor

$$W=20\left(\frac{\text{Vol}}{\text{Vol}_{\min}}\right)^{1/3} \tag{18}$$

where $\text{Vol}_{\min}$ represents the minimum volume within the computational domain. Computational time for the inviscid computations is 7.7×10^{-6} CPU s/grid point/time step on the CRAY-1 computer.

Viscous-Inviscid Interaction

It is convenient in the viscous-inviscid iteration process to keep the computational mesh used in the finite-volume Euler equation solution fixed. Therefore, the surface source model is convenient because a surface source mass flux is imposed as a boundary condition in the inviscid calculation at the physical body surface, and hence avoids mesh adjustment during the iteration as would be required in the effective displacement surface approach, for example.

The idea of a surface source model seems to have originated with Lighthill[9] in what he refers to as the method of equivalent sources. Lock[10] and Carter,[8] among others, have used this method for viscous-inviscid iterative calculations. In this method, the influence of viscous flow on inviscid flow is accounted for by replacing the normal wall boundary condition of $\boldsymbol{q}\cdot\boldsymbol{n}=0$ with $\boldsymbol{q}\cdot\boldsymbol{n}=v_n$ in the inviscid calculation. Because the inviscid calculation method used herein is conservative, the actual surface boundary condition imposed in the inviscid calculation is $\rho\boldsymbol{q}\cdot\boldsymbol{n}=(\rho v)_n$, where $(\rho v)_n$ is obtained from

$$(\rho v)_n=\frac{1}{r_w^k}\frac{\mathrm{d}(\rho_e u_e r_w^k \delta^*)}{\mathrm{d}x} \tag{19}$$

where $k=0$ for two-dimensional flow and $k=1$ for axisymmetric flow.

The term $(\rho v)_n$ is updated in the iteration cycle as follows. The δ^* distribution from the previous iteration is used (initially a flat plate δ^* distribution is used) in the inverse boundary-layer code to solve for the distribution of $\rho_e u_e \delta^*$. This quantity is then used in Eq. (19) to calculate $(\rho v)_n$ for the next inviscid calculation. The δ^* distribution for the next viscous calculation is obtained from the idea of Carter.[8] The expression used is

$$\delta^{*\,(\eta+1)}=\delta^{*\,(\eta)}\frac{u_{e,v}}{|q_{w,i}|} \tag{20}$$

where $u_{e,v}$ is the distribution of the boundary-layer edge velocity obtained from the last viscous solution, and $|q_{w,i}|$ is the distribution of the magnitude of the velocity vector at the surface obtained from the last inviscid solution. Convergence is monitored by noting the change in δ^*. For a typical viscous-inviscid interaction solution where convergence is obtained in about 8000 iterations, an inverse boundary-layer solution is obtained about every 400 iterations.

Results and Discussion

Calculations using the present viscous-inviscid interaction calculation method are compared with four sets of experimental transonic flow data. These data sets include the shock/boundary-layer interaction data of Altstatt,[21] the 18% thick circular-arc airfoil data reported by Deiwert,[22] the equivalent body of revolution data of Smith,[23] and the experiment of three MK-83 stores in a TER configuration of Heltsley and Cline.[24]

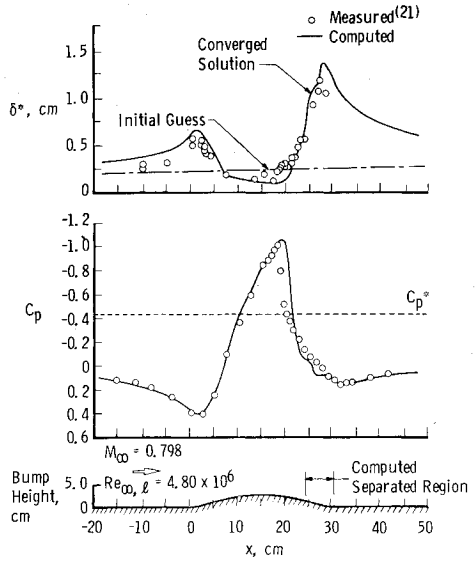

Fig. 6 Computed and measured surface pressure and boundary-layer displacement thickness distributions of transonic flow over a bump.

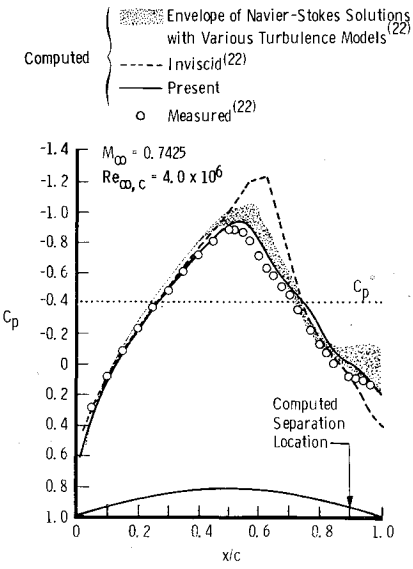

Fig. 7 Computed and measured surface pressure distributions of transonic flow over an 18%-thick circular-arc airfoil.

The experiment of Altstatt[21] involves the transonic flow over a 2.54-cm high, 30.48-cm long bump located on the wall of a 30.48-cm^2 perforated wall wind tunnel. Surface static pressure, laser velocimeter, and pitot pressure measurements were made for $M_\infty=0.798$ and $Re_{\infty,c}=4.8\times10^6$. Comparisons of calculated and measured surface pressure coefficients and boundary-layer displacement thickness distributions are presented in Fig. 6. Reasonably good agreement between calculated and measured data is indicated. Included in Fig. 6 is the flat plate boundary-layer displacement thickness distribution used as an initial condition to begin the viscous calculations.

Deiwert[22] compared Reynolds averaged Navier-Stokes calculations with surface pressure measurements of transonic flow over an 18% thick circular-arc airfoil. Comparisons of the present calculations with these experimental data, and the calculations of Deiwert for $M_\infty=0.7425$ and $Re_{\infty,c}=4\times10^6$ are presented in Fig. 7. Deiwert investigated various turbulence models, the results of which are indicated by the shaded area. The present calculations give about the same quality of agreement with the experimental pressure data as Deiwert's calculations. Shadowgraphs presented in Ref. 22

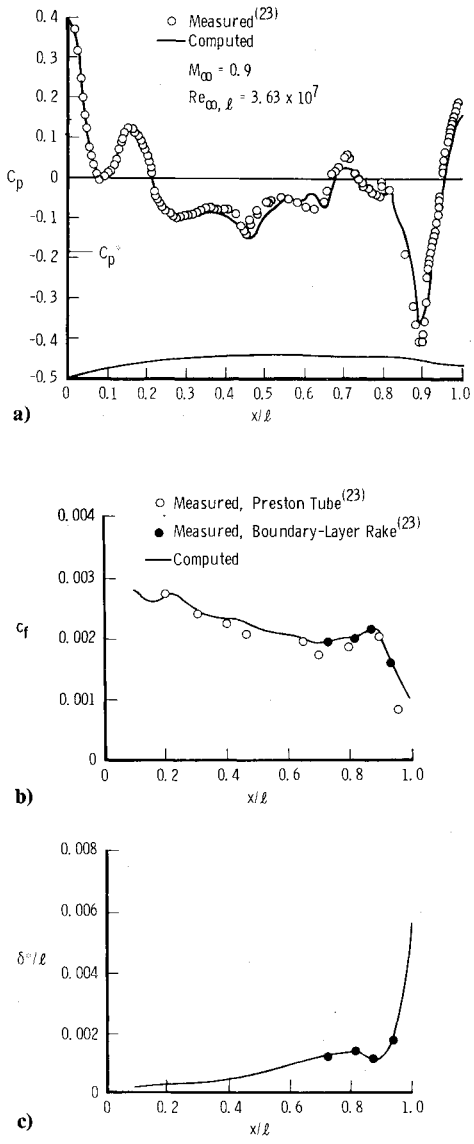

Fig. 8 Computed and measured a) surface pressure, b) skin friction, and c) displacement thickness distribution for transonic flow over a body of revolution.

are said to indicate that the boundary layer remains attached behind the shock (which was located at 63% chord) with substantial thickening, and finally separation near the trailing edge. The boundary-layer separation point was at 90% chord according to the present computations. The conditions routinely imposed for starting the boundary-layer solution at some assumed transition location, in this case at 2% chord, are $\bar{H} = 1.5$ and $\overline{Re_\theta} = 500$.

The experiment of Smith[23] involves the transonic flow over an axisymmetric body of revolution with continuous axial variations in cross-sectional area. Detailed surface pressure measurements are available along with some skin friction and boundary-layer rake measurements. Calculated and measured surface pressure coefficients, local skin friction coefficients, and boundary-layer displacement thickness distributions are compared in Fig. 8 for $M_\infty = 0.9$ and $Re_{\infty,\ell} = 3.63 \times 10^7$. The agreement is considered good. The flow did not separate, although it is near separation near the rear of the body.

The experiment of Heltsley and Cline[24] involved the surface static pressure and laser velocimeter measurements of the transonic flow about three MK-83 stores arranged in a triple-ejection-rack (TER) configuration. This computational test case is important because it clearly demonstrates the power of the Euler equation code, and also an assessment can

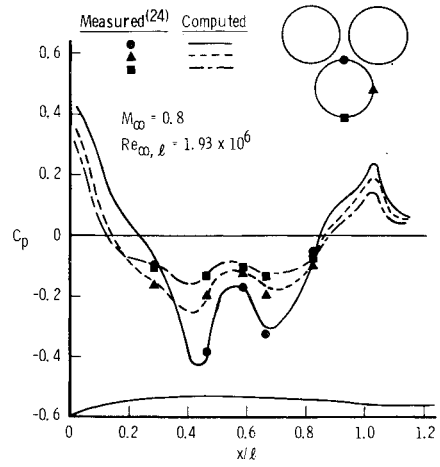

Fig. 9 Computed and measured surface pressure distributions for transonic flow about three stores in a TER configuration.

be made of the quality of results that might be obtained for practical three-dimensional problems by coupling a two-dimensional inverse boundary-layer code with a three-dimensional inviscid code. Interacting inverse boundary-layer solutions were obtained along the surface of the stores in the streamwise direction at circumferential locations corresponding to the finite-volume cell centers where inviscid flow properties are computed and the inviscid wall source fluxes are imposed. It is stressed that cross-flow viscous effects are not taken into account properly. Rather, the viscous effects are those resulting from streamwise pressure gradients, and variations thereof, circumferentially around the stores. However, the present method allows estimates of the friction drag to be obtained in mildly three-dimensional flows without resorting to fully three-dimensional viscous solutions. Calculated and measured streamwise surface pressure coefficients at three circumferential locations, are compared in Fig. 9 for $M_\infty = 0.8$ and $Re_{\infty,\ell} = 1.93 \times 10^6$. The flow is slightly supercritical in the interior of this store arrangement. The agreement in Fig. 9 is considered good.

Concluding Remarks

The inverse turbulent boundary-layer integral method presented differs from other methods primarily in that a new analytical turbulent boundary-layer velocity profile expression is used for attached and separated flow. The code used for inviscid flow calculations is a fully conservative, time-dependent, three-dimensional, finite volume, Euler equation code. The viscous and inviscid flows are coupled using the surface source model and the iteration procedure used to update the displacement thickness distribution in the inverse boundary-layer calculations is the method of Carter.[8]

All calculations presented were performed on a CRAY-1 computer. Depending on the mesh and the strength of the viscous-inviscid interaction, solution times varied from 2 to 6 min. For the three-dimensional solution of flow about three MK-83 stores in a TER configuration, a $41 \times 20 \times 5$ mesh was used. An inviscid solution was obtained in 2 min in 3000 time steps using a CFL number of 0.8, and a viscous-inviscid interaction solution was obtained in 3 min in 4400 time steps using a CFL number of 0.8, with a viscous solution obtained every 400 time steps. This solution indicates that practical results for a three-dimensional transonic viscous-inviscid interacting flow can be obtained in a reasonable amount of time and cost using the present method on an advanced computer.

References

[1] Brown, S. N. and Stewartson, K., "Laminar Separation," *Annual Review of Fluid Mechanics*, Vol. 1, 1969, pp. 45-72.

[2] Catherall, D. and Mangler, K. W., "The Integration of the Two-Dimensional Laminar Boundary-Layer Equations Past the Point of Vanishing Skin Friction," *Journal of Fluid Mechanics*, Vol. 26, Pt. 1, 1966, pp. 163-183.

[3] Kuhn, G. D. and Nielsen, J. N., "Prediction of Turbulent Separated Boundary Layers," AIAA Paper 73-663, July 1973.

[4] Thiede, P. G., "Prediction Method for Steady Aerodynamic Loading on Airfoils with Separated Transonic Flow," AGARD CP-204, *Prediction of Aerodynamic Loading*, Sept. 1976.

[5] East, L. F., Smith, P. D., and Merryman, P. J., "Prediction of the Development of Separated Turbulent Boundary Layers by the Lag-Entrainment Method," Royal Aeronautical Establishment, Farnborough, Hants, U.K., RAE TR 77046, 1977.

[6] Carter, J. E., "Inverse Boundary-Layer Theory and Comparison with Experiment," NASA TP 1208, 1978.

[7] Kuhn, G. D., "Calculation of Separated Turbulent Flows on Axisymmetric Afterbodies Including Exhaust Plume Effects," *AIAA Journal*, Vol. 18, March 1980, pp. 235-242.

[8] Carter, J. E., "A New Boundary-Layer Inviscid Iteration Technique for Separated Flow," AIAA Paper 79-1450, July 1979.

[9] Lighthill, M. J., "On Displacement Thickness," *Journal of Fluid Mechanics*, Vol. 4, Pt. 4, 1958, pp. 383-392.

[10] Lock, R. C., "Calculation of Viscous Effects on Aerofoils in Compressible Flow," Royal Aeronautical Establishment, Farnborough, Hants, U.K., RAE TM Aero 1646, Sept. 1975.

[11] Whitfield, D. L., "Integral Solution of Compressible Turbulent Boundary Layers Using Improved Velocity Profiles," Arnold Air Force Station, Tenn., AEDC-TR-78-42, Dec. 1978.

[12] Whitfield, D. L., "Analytical Description of the Complete Turbulent Boundary-Layer Velocity Profile," *AIAA Journal*, Vol. 17, Oct. 1979, pp. 1145-1147.

[13] Swafford, T. W., "Analytical Approximation of Two-Dimensional Separated Turbulent Boundary-Layer Velocity Profiles," Arnold Air Force Station, Tenn., AEDC-TR-79-99, Oct. 1980.

[14] Simpson, R. L., Strickland, J. H., and Barr, P. W., "Features of a Separating Turbulent Boundary Layer in the Vicinity of Separation," *Journal of Fluid Mechanics*, Vol. 79, March 1977, pp. 553-594.

[15] Alber, I. E., Bacon, J. W., Masson, B. S., and Collins, D. J., "An Experimental Investigation of Turbulent Transonic Viscous-Inviscid Interactions," *AIAA Journal*, Vol. 11, May 1972, pp. 620-627.

[16] Coles, D. E. and Hirst, E. A., eds., *Proceedings, Computation of Turbulent Boundary Layers—1968 AFOSR-IFP-Stanford Conference*, Vol. II, Stanford University Press, Stanford, Calif., 1968.

[17] White, F. M., *Viscous Fluid Flow*, McGraw-Hill Book Co., Inc., New York, 1974.

[18] Cebeci, T. and Smith, A.M.O., *Analysis of Turbulent Boundary Layers*, Academic Press, New York, 1974.

[19] Chu, J. and Young, A. D., "Characteristics of a Separated Incompressible Turbulent Boundary Layer," AGARD CP-168, Paper 13, 1976.

[20] MacCormack, R. W., "The Effect of Viscosity in Hypervelocity Impact Cratering," AIAA Paper 69-354, May 1969.

[21] Altstatt, M. C., "An Experimental and Analytical Investigation of a Transonic Shock-Wave/Boundary-Layer Interaction," Arnold Air Force Station, Tenn., AEDC-TR-77-47, May 1977.

[22] Deiwert, G. S., "Computation of Separated Transonic Turbulent Flows," *AIAA Journal*, Vol. 14, June 1976, pp. 735-740.

[23] Smith, C. L., "Skin Friction Measurements at Transonic Mach Numbers," Arnold Air Force Station, Tenn., AEDC-TSR-79-P62, Oct. 1979.

[24] Heltsley, F. L. and Cline, V. A., "Wing/Store Flow Field Measurements at Transonic Speeds Using a Laser Velocimeter," Arnold Air Force Station, Tenn., AEDC-TR-79-5, April 1979.